Normal and tangential stiffnesses of rough surfaces in contact via an imperfect interface model

Maria Letizia Raffa, Frédéric Lebon, Giuseppe Vairo

Normal and tangential stiffnesses of rough surfaces in contact via an imperfect interface model

Maria Letizia Raffa[a,b,*], Frédéric Lebon[a], Giuseppe Vairo[b]

[a] LMA, Aix-Marseille University, CNRS, Centrale Marseille, 4 Impasse Nikola Tesla CS 40006, 13453 Marseille Cedex 13, France
[b] Department of Civil Engineering and Computer Science Engineering (DICII), University of Rome "Tor Vergata", via del Politecnico 1, 00133 Rome, Italy

In this paper a spring-like micromechanical contact model is proposed, aiming to describe the mechan- ical behavior of two rough surfaces in no-sliding contact under a closure pressure. The contact region between two elastic bodies is described as a thin damaged interphase characterized by the occurrence of non-interacting penny-shaped cracks (*internal* cracks). By combining a homogenization approach and an asymptotic technique, tangential and normal equivalent contact stiffnesses are consistently derived. An analytical description of evolving contact and no-contact areas with respect to the closure pressure is also provided, resulting consistent with theoretical Hertz-based asymptotic predictions and in good agreement with available numerical estimates. Proposed model has been successfully validated through comparisons with some theoretical and experimental results available in literature, as well as with other well-established modeling approaches. Finally, the influence of main model parameters is addressed, proving also the model capability to catch the experimentally-observed dependence of the tangent-to- normal contact stiffness ratio on the closure pressure.

Keywords: Interface contact stiffness, Contact area, Imperfect interface approach Homogenization of a microcracked interphase, Asymptotic analysis

1. Introduction

Analytical and numerical modeling of contact problems related to rough surfaces can be surely considered as an open and challenging research topic, strictly associated to many applications in different engineering fields. From a computational point of view, it is possible to identify a class of modeling problems in which it is neither possible nor convenient to account for a fine and detailed description of the contact regions, although local contact features may strongly affect the overall mechanical response for the problem under investigation. In these cases, a possible strategy is based on modeling contact scenarios by introducing suitable stiffness and dashpot distributions at the contact nominal interface, allowing to upscale at the macroscale the influence of dominant contact mechanisms occurring at the roughness scale. In this context and as reviewed by Baltazar et al. (2002), starting from fundamental results of classic contact theories and accounting for main microgeometric features at the contact interface, several theoretical and numerical models have been proposed in the specialized literature (namely, spring-like models), aiming to consistently derive some equivalent stiffnesses.

One of the earliest contact model for elastic rough surfaces was proposed by Greenwood and Williamson (1966). This model is based on the Hertz contact solution for curved elastic nominally-flat surfaces (Mindlin, 1949) and it accounts for a statistical distribution of non-interacting asperities. Moreover, Yoshioka and Scholz (1989) proposed an elastic contact model via a statistical approach that allows to describe possible oblique contact conditions among asperities. By combining the Hertz–Mindlin theory (Mindlin, 1949) and the previously-introduced Greenwood-Williamson contact model, Sherif and Kossa (1991) and Krolikowski and Szczepek (1993) provided an analytical description of normal and tangential contact stiffnesses, in order to establish a theoretical interpretation for the experimental results they obtained. In this case, the contact between two nominally-flat rough surfaces is modeled as the contact between two elastic surfaces, one of which is ideally flat and the other is nominally flat but covered with many spherically-shaped asperities. A generalization of such an approach was developed by Baltazar et al. (2002), accounting also for a possible contact misalignment. Nevertheless, a possible common drawback of all the aforementioned contact models is that they are generally based on a stochastic approach. Accordingly, in order to

* Corresponding author at: LMA - CNRS UPR 7051, Aix-Marseille University, 4 Impasse Nikola Tesla CS 40006 -13453 Marseille Cedex 13, France. Tel.: +33 6 34 14 13 59.

E-mail addresses: raffa@ing.uniroma2.it, raffa@lma.cnrs-mrs.fr (M.L. Raffa), lebon@lma.cnrs-mrs.fr (F. Lebon), vairo@ing.uniroma2.it (G. Vairo).

make them practically applicable, the identification of a number of statistic parameters, often not easily estimable (McCool, 1986), is required.

A crucial aspect in deriving reliable contact solutions is related to the description of the contact area and its evolution with respect to the closure pressure (Johnson, 1987). Starting from the analytical solution of Westergaard (1939), Johnson et al. (1985) developed a model for the elastic contact between a two-dimensional wavy surface and a rigid flat plane, proposing an analytic description of the contact area in the asymptotic limit cases of early contact (namely, for small values of the closure pressure) and of nearly-full contact conditions (high values of the closure pressure). More recently, Yastrebov et al. (2014) proposed a refined numerical approach consisting in a FFT-based boundary-element formulation, and they obtained an accurate numerical description of the contact-area evolution with the closure pressure in the case of the elastic contact between a wavy surface and a flat plane.

Several experimental studies can be found in the literature addressing the mechanical behavior of rough surfaces in no-sliding contact under closure-pressure conditions (e.g., Krolikowski et al., 1989; Sherif and Kossa, 1991; Krolikowski and Szczepek, 1993; Baltazar et al., 2002; Dwyer-Joyce and Gonzalez-Valadez, 2003; Gonzalez-Valadez et al., 2010), providing also estimates for normal and tangential contact stiffnesses. For instance, Krolikowski and coworkers (Krolikowski and Szczepek, 1993; Krolikowski et al., 1989) proposed contact-stiffness measures through an ultrasonic method, based on the measurement of the reflection coefficient of ultrasonic waves at the contact interface. Sherif and Kossa (1991) employed an experimental technique based on the evaluation of the local natural frequencies at the contact region. Gonzalez-Valadez et al. (2010) proposed results based on ultrasonic tests and accounting also for loading-unloading cycles of the closure pressure. As a matter of fact, experimental results confirm that: high stress concentrations appear at the contact region, and they result practically unaffected by the shape of bodies in contact at a suitable distance from the contact area (Johnson, 1987; Johnson et al., 1985); hysteresis phenomena occur at the interface (as a result of the plastic deformation localized at the asperity tips) in the case of cycling loads (Gonzalez-Valadez et al., 2010); null values of interface stiffnesses are achieved when the closure pressure tends to zero (Gonzalez-Valadez et al., 2010).

In this paper a novel spring-like theoretical model for no-sliding contact under a closure pressure is proposed. Incremental normal and tangential equivalent stiffnesses at the nominal contact interface are derived, by assuming contact microgeometry be described by isolated *internal* cracks (Sevostianov and Kachanov, 2008a; 2008b) occurring in a thin interphase region. In detail, effective mechanical properties at the contact zone are consistently derived following the imperfect interface approach recently adopted by Lebon and coworkers (Fouchal et al., 2014; Rekik and Lebon, 2010; 2012), by coupling a homogenization approach for microcracked media based on the non-interacting approximation (Kachanov, 1994; Kachanov and Sevostianov, 2005; Sevostianov and Kachanov, 2013; Tsukrov and Kachanov, 2000) and the matched asymptotic expansion method, introduced by Sanchez-Palencia (1987) and Sanchez-Palencia and Sanchez-Hubert (1992) and recently employed by Lebon and Rizzoni (2011), Rizzoni and Lebon (2013), Rizzoni et al. (2014) and Lebon and Zaittouni (2010).

The proposed model is detailed in Section 2, and its validation is provided by comparing numerical results with available theoretical and experimental findings (Section 3.1). Model effectiveness is also proved for a wide range of closure-pressure values by comparing proposed results with those obtained via the contact model introduced by Sherif and Kossa (1991) (Section 3.2). Afterwards, the influence of main model parameters is investigated in Section 3.3, and finally some conclusions are traced in Section 4.

2. Contact model

2.1. General framework

Let the contact problem $\mathcal{C}$ be introduced by considering two continuous bodies Ω_1 and Ω_2, comprising linearly-elastic isotropic materials (E_i and ν_i, with $i = 1, 2$, being Young modulus and Poisson ratio, respectively), in no-sliding contact via non-conforming rough surfaces under a closure pressure condition (Fig. 1). Let $\mathcal{S} \subset \mathbb{R}^2$ be the nominal contact interface, belonging to the interface plane π. Let a Cartesian frame (O, $\mathbf{e}_1$, $\mathbf{e}_2$, $\mathbf{e}_3$) be introduced, with x_1, x_2 and x_3 the corresponding coordinates. The origin O belongs to π, and $\mathbf{e}_3$ is orthogonal to π and directed outward from Ω_2.

Normal and tangential incremental contact stiffnesses ($K_N^{\mathcal{C}}$ and $K_T^{\mathcal{C}}$, respectively) per unit nominal contact area in $\mathcal{S}$ are defined as:

$$K_N^{\mathcal{C}} = \frac{\mathrm{d}\mathcal{F}_N}{\mathrm{d}w}, \quad K_T^{\mathcal{C}} = \frac{\mathrm{d}\mathcal{F}_T}{\mathrm{d}s} \tag{1}$$

where $\mathrm{d}w$ and $\mathrm{d}s$ are the increments of the relative displacements at the contact interface region in normal (i.e., along $\mathbf{e}_3$) and tangential (i.e., parallel to π) directions, and $\mathrm{d}\mathcal{F}_N$ and $\mathrm{d}\mathcal{F}_T$ are the increments of the normal and tangential forces transmitted through the unit contact area, respectively. Contact microgeometry is assumed to be isotropic in $\mathcal{S}$ and thereby the tangential contact stiffness $K_T^{\mathcal{C}}$ can be postulated as independent from the tangential direction.

In agreement with the approach adopted by Westergaard (1939) and by Johnson et al. (1985), contact microgeometry is modeled by describing no-contact regions as parallel penny-shaped *internal* cracks (Sevostianov and Kachanov, 2008a; 2008b) lying on the interface plane π. Coplanar mechanical interactions among cracks are considered negligible, resulting in the non-interacting approximation (Kachanov, 1994; Sevostianov and Kachanov, 2013). Accordingly, the region close to the nominal contact interface $\mathcal{S}$ is regarded as an imperfect interphase $\mathcal{B}^\varepsilon$, defined as the thin layer having $\mathcal{S}$ as the middle section and ε as the uniform small thickness, and weakened by identical and parallel penny-shaped cracks of radius b (Fig. 1).

Referring to a simplistic idealization of the contacting rough surfaces via bi-sinusoidal wavy-like smooth surfaces, both of them with wavelength λ and amplitude Δ (such that $\Delta \ll \lambda$), a ε-thick representative elementary volume (REV) at the contact interface, and occupying the region $\Delta\Omega^\varepsilon \subset \mathcal{B}^\varepsilon$, can be conveniently introduced as sketched in Fig. 1.

Accordingly, the contact problem $\mathcal{C}$ is faced by introducing an auxiliary model problem $\mathcal{A}$, defined on the microcracked interphase $\mathcal{B}^\varepsilon$ and described via the REV.

2.2. Imperfect interface approach

Referring to the auxiliary model problem $\mathcal{A}$, and as a notation rule, the following symbols will be adopted: $\Omega_+^\varepsilon = \Omega_1 \setminus \mathcal{B}^\varepsilon$ and $\Omega_-^\varepsilon = \Omega_2 \setminus \mathcal{B}^\varepsilon$, with $\Omega_\pm^\varepsilon$ also referred to as adherents; $\mathcal{S}_\pm^\varepsilon = \Omega_\pm^\varepsilon \cap \mathcal{B}^\varepsilon$ identifying the plane interfaces parallel to π between interphase and adherents. It is assumed that $\Omega_\pm^\varepsilon$ and $\mathcal{B}^\varepsilon$ are perfectly bonded, so that displacement and stress vector fields are ensured to be continuous across $\mathcal{S}_\pm^\varepsilon$.

2.2.1. Homogenization of the microcracked interphase

Let $\Gamma \subset \mathcal{S}$ be the crack middle surface for a penny-shaped crack in $\mathcal{B}^\varepsilon$, and let $\mathbf{u}^+$ and $\mathbf{u}^-$ be the displacement vectors at the parallel-to-$\mathcal{S}$ crack boundaries. Denote also with $\mathbf{u}_{\mathrm{cod}} = \int_\Gamma (\mathbf{u}^+ - \mathbf{u}^-)\mathrm{d}\Gamma/|\Gamma|$ the average measure of the displacement jump across the crack, in the following referred to as the crack opening displacement vector. In agreement with a well-established

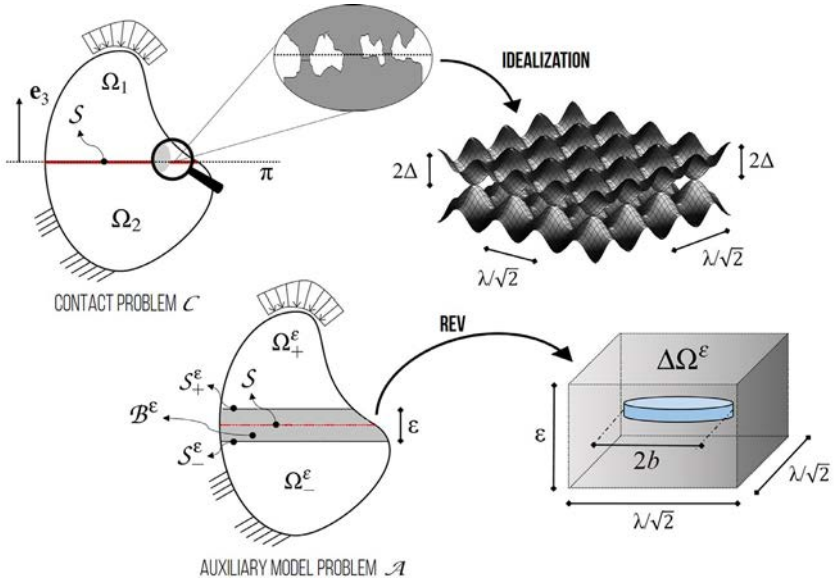

Fig. 1. Contact problem $\mathcal{C}$ and auxiliary model problem $\mathcal{A}$. Notation.

homogenization technique (Kachanov, 1994; Kachanov and Sevostianov, 2005; Tsukrov and Kachanov, 2000), and considering a plane-stress assumption under a frictionless condition along the crack faces, $\mathbf{u}_{\text{cod}}$ can be expressed in terms of the stress vector $\mathbf{t}_3 = \boldsymbol{\sigma}\,\mathbf{e}_3$ as (Kachanov, 1994):

$$\mathbf{u}_{\text{cod}} = \beta \frac{b}{E_0} \mathbf{P}_3\,\mathbf{t}_3 + \gamma \frac{b}{E_0} (\mathbf{I} - \mathbf{P}_3)\,\mathbf{t}_3 \tag{2}$$

where $\boldsymbol{\sigma}$ is the second-order Cauchy stress tensor, $\mathbf{P}_3 = \mathbf{e}_3 \otimes \mathbf{e}_3$ is the projector operator along $\mathbf{e}_3$ (symbol '$\otimes$' indicating the dyadic product), $\mathbf{I}$ is the identity second-order tensor, and where

$$\beta = \frac{16(1-\nu_0^2)}{3\pi}, \quad \gamma = \frac{32(1-\nu_0^2)}{3\pi\,(2-\nu_0)} \tag{3}$$

E_0 and ν_0 being, respectively, the Young modulus and the Poisson ratio of the undamaged interphase, assumed to be isotropic. It is worth pointing out that E_0 and ν_0 can be obtained in terms of the elastic properties (E_i and ν_i, with $i = 1, 2$) of the two materials in contact, as the result of a preliminary homogenization step performed on the undamaged ε-thick REV (e.g., Sanchez-Palencia, 1980; Nemat-Nasser and Hori, 2013; Temizer and Wriggers, 2011). Following the Eshelby approach (Eshelby, 1961), the complementary elastic potential $\psi(\boldsymbol{\sigma})$ characterizing the effective material of the microcracked interphase results in:

$$\psi(\boldsymbol{\sigma}) = \psi_0 + \Delta\psi = \frac{1}{2}\boldsymbol{\sigma} : \mathbb{S}_0 : \boldsymbol{\sigma} + \frac{|\Gamma|}{2\,|\Delta\Omega^\varepsilon|}\boldsymbol{\sigma} : (\mathbf{e}_3 \otimes \mathbf{u}_{\text{cod}}) \tag{4}$$

where symbol ': ' denotes the double-dot product, $\psi_0(\boldsymbol{\sigma})$ is the complementary potential expressed in terms of the fourth-order compliance tensor $\mathbb{S}_0 = \mathbb{S}_0(E_0, \nu_0)$ of the undamaged interphase, and $\Delta\psi$ is a perturbation term, depending on both microstructural crack features and the crack opening displacement.

By introducing Eqs. (2) and (3) in Eq. (4), the complementary elastic potential $\psi(\boldsymbol{\sigma})$ of the cracked material in $\mathcal{B}^\varepsilon$ reads as (Kachanov and Sevostianov, 2005):

$$\psi = \psi_0 + \frac{16(1-\nu_0^2)}{3(2-\nu_0)E_0}\left\{(\boldsymbol{\sigma}\,\boldsymbol{\sigma}) : \boldsymbol{\alpha} - \frac{\nu_0}{2}\boldsymbol{\sigma} : (\boldsymbol{\alpha} \otimes \mathbf{P}_3) : \boldsymbol{\sigma}\right\} \tag{5}$$

where the complementary elastic potential of the undamaged interphase is expressed by

$$\psi_0(\boldsymbol{\sigma}) = \frac{1+\nu_0}{2E_0}\boldsymbol{\sigma} : \boldsymbol{\sigma} - \frac{\nu_0}{2E_0}\boldsymbol{\sigma} : \mathbf{I} \tag{6}$$

and $\boldsymbol{\alpha} = \rho\,\mathbf{P}_3$ is the second-order crack-density tensor, expressed in terms of the scalar density ρ. The latter is defined, in agreement with Bristow (1960), by (see Fig. 1):

$$\rho = \frac{b^3}{|\Delta\Omega^\varepsilon|} = \frac{2b^3}{\lambda^2\varepsilon} \tag{7}$$

Due to Eq. (5), the effective compliance tensor $\mathbb{S}$ of the microcracked interphase can be derived component-wise as:

$$(\mathbb{S})_{ijkl} = (\mathbb{S}_0)_{ijkl} + (\Delta\mathbb{S})_{ijkl} = \frac{\partial^2\psi}{\partial\sigma_{ij}\partial\sigma_{kl}} \tag{8}$$

where $\Delta\mathbb{S}$ is the part of the compliance tensor associated to $\Delta\psi$. As a result, the damaged interphase behaves as a transversely isotropic material, with symmetry plane coincident with the interphase mid-plane (namely, π). Therefore, by discriminating with indexes N and T quantities referred to normal and tangential directions to π, respectively, the effective moduli of the cracked interphase result in:

$$E_N = E_0\left\{1+\frac{16(1-\nu_0^2)}{3}\,\rho\right\}^{-1}, \quad E_T = E_0\left\{1+\frac{16\nu_0(1-\nu_0^2)}{3(2-\nu_0)}\,\rho\right\}^{-1}$$
$$G_{NT} = G_0\left\{1+\frac{16(1-\nu_0)}{3(2-\nu_0)}\,\rho\right\}^{-1}, \quad \nu_{NT} = \nu_0\left\{1+\frac{16\nu_0(1-\nu_0^2)}{3(2-\nu_0)}\,\rho\right\}^{-1}$$
$$\nu_{TN} = \nu_0\left\{1+\frac{16(1-\nu_0^2)}{3}\,\rho\right\}^{-1} \tag{9}$$

where symbol $G_{\cdot}$ indicates shear moduli.

2.2.2. Asymptotic analysis

Let the interphase thickness ε (see Fig. 1) be considered as a small parameter. Accordingly, an asymptotic expansion with respect to ε can be conveniently performed referring to the composite system $\Omega^\varepsilon = \Omega^\varepsilon_+ \cup \Omega^\varepsilon_- \cup \mathcal{B}^\varepsilon$, where the mechanical properties of the adherents are those of the bodies Ω_1 and Ω_2 in contact, and with the effective material properties of the interphase $\mathcal{B}^\varepsilon$ given by Eq. (9).

In agreement with Ciarlet (1997), let the change of variable $\hat{\mathbf{g}}$: $(x_1, x_2, x_3) \to (z_1, z_2, z_3)$ be introduced in $\mathcal{B}^\varepsilon$, with $z_1 = x_1$, $z_2 = x_2$, $z_3 = x_3/\varepsilon$. Moreover, let the change of variable $\bar{\mathbf{g}}$: $(x_1, x_2, x_3) \to (z_1, z_2, z_3)$ be introduced in $\Omega^\varepsilon_\pm$, with $z_1 = x_1$, $z_2 = x_2$, $z_3 = x_3 \pm (1-\varepsilon)/2$, where the plus (resp., minus) sign applies for Ω^ε_+ (resp.,

Ω^ε_-). As a result, interphase $\mathcal{B}^\varepsilon$ and adherents $\Omega^\varepsilon_\pm$ are rescaled in $\mathcal{B} = \left\{(z_1, z_2, z_3) \in \mathbb{R}^3 \mid (z_1, z_2) \in \mathcal{S},\ |z_3| < 1/2\right\}$ and $\Omega_\pm = \Omega^\varepsilon_\pm \pm (1-\varepsilon)\mathbf{e}_3/2$, respectively. In what follows, symbols '$\hat{\cdot}$' and '$\bar{\cdot}$' refer to rescaled quantities for $\mathcal{B}$ and $\Omega_\pm$, respectively. In detail, $\hat{\mathbf{u}}^\varepsilon = \mathbf{u}^\varepsilon \circ \hat{\mathbf{g}}^{-1}$ and $\hat{\boldsymbol{\sigma}}^\varepsilon = \boldsymbol{\sigma}^\varepsilon \circ \hat{\mathbf{g}}^{-1}$ denote displacement and stress fields for $\mathcal{B}$, and $\bar{\mathbf{u}}^\varepsilon = \mathbf{u}^\varepsilon \circ \bar{\mathbf{g}}^{-1}$ and $\bar{\boldsymbol{\sigma}}^\varepsilon = \boldsymbol{\sigma}^\varepsilon \circ \bar{\mathbf{g}}^{-1}$ are displacement vector and stress tensor for $\Omega_\pm$, $\mathbf{u}^\varepsilon$ and $\boldsymbol{\sigma}^\varepsilon$ being the corresponding fields on the composite system Ω^ε. Accordingly, displacement and stress asymptotic expansions with respect to the small thickness ε result, respectively, in:

$$\begin{aligned}
\mathbf{u}^\varepsilon &= \mathbf{u}^0 + \varepsilon\,\mathbf{u}^1 + \mathrm{o}(\varepsilon)\\
\hat{\mathbf{u}}^\varepsilon &= \hat{\mathbf{u}}^0 + \varepsilon\,\hat{\mathbf{u}}^1 + \mathrm{o}(\varepsilon)\\
\bar{\mathbf{u}}^\varepsilon &= \bar{\mathbf{u}}^0 + \varepsilon\,\bar{\mathbf{u}}^1 + \mathrm{o}(\varepsilon)
\end{aligned} \tag{10}$$

$$\begin{aligned}
\boldsymbol{\sigma}^\varepsilon &= \boldsymbol{\sigma}^0 + \varepsilon\,\boldsymbol{\sigma}^1 + \mathrm{o}(\varepsilon)\\
\hat{\boldsymbol{\sigma}}^\varepsilon &= \hat{\boldsymbol{\sigma}}^0 + \varepsilon\,\hat{\boldsymbol{\sigma}}^1 + \mathrm{o}(\varepsilon)\\
\bar{\boldsymbol{\sigma}}^\varepsilon &= \bar{\boldsymbol{\sigma}}^0 + \varepsilon\,\bar{\boldsymbol{\sigma}}^1 + \mathrm{o}(\varepsilon)
\end{aligned} \tag{11}$$

and, due to Eq. (10), strain tensor in the rescaled domains takes the form (Rizzoni et al., 2014):

$$\mathbf{e}(\hat{\mathbf{u}}^\varepsilon) = \varepsilon^{-1}\hat{\mathbf{e}}^{-1} + \hat{\mathbf{e}}^0 + \mathrm{O}(\varepsilon) \tag{12}$$

$$\mathbf{e}(\bar{\mathbf{u}}^\varepsilon) = \varepsilon^{-1}\bar{\mathbf{e}}^{-1} + \bar{\mathbf{e}}^0 + \mathrm{O}(\varepsilon) \tag{13}$$

where the lower-order terms are

$$\hat{\mathbf{e}}^{-1} = \frac{\hat{\mathbf{u}}^0_{,3} \otimes \mathbf{e}_3 + \mathbf{e}_3 \otimes \hat{\mathbf{u}}^0_{,3}}{2}, \qquad \bar{\mathbf{e}}^{-1} = \mathbf{0} \tag{14}$$

$f_{,3}$ denoting the partial derivative of f with respect to z_3, with $f_{,3} = \varepsilon\,\partial f/\partial x_3$ in the interphase domain.

Owing the perfect bonded assumption between $\mathcal{B}^\varepsilon$ and $\Omega^\varepsilon_\pm$, the continuity condition at $\mathcal{S}^\varepsilon_\pm$ for the fields $\mathbf{u}^\varepsilon$ and $\boldsymbol{\sigma}^\varepsilon$ leads to matching relationships between external and internal expansions. In particular, zero-order terms have to satisfy the following conditions:

$$\mathbf{u}^0\left(x_1, x_2, 0^\pm\right) = \hat{\mathbf{u}}^0\left(z_1, z_2, \pm\frac{1}{2}\right) = \bar{\mathbf{u}}^0\left(z_1, z_2, \pm\frac{1}{2}\right) \tag{15}$$

$$\mathbf{t}^0_3\left(x_1, x_2, 0^\pm\right) = \hat{\mathbf{t}}^0_3\left(z_1, z_2, \pm\frac{1}{2}\right) = \bar{\mathbf{t}}^0_3\left(z_1, z_2, \pm\frac{1}{2}\right) \tag{16}$$

where $\mathbf{u}^\varepsilon \to \mathbf{u}^0$ and $\mathbf{t}^\varepsilon_3 = \boldsymbol{\sigma}^\varepsilon\,\mathbf{e}_3 \to \mathbf{t}^0_3 = \boldsymbol{\sigma}^0\,\mathbf{e}_3$ when $\varepsilon \to 0$.

It is worth pointing out that, neglecting body forces in the interphase $\mathcal{B}^\varepsilon$, and as a result of the rescaled equilibrium problem in $\mathcal{B}$ (Rizzoni et al., 2014), the zero-order stress field $\hat{\boldsymbol{\sigma}}^0$ is such that the stress vector $\hat{\mathbf{t}}^0_3 = \hat{\boldsymbol{\sigma}}^0\,\mathbf{e}_3$ does not depend on z_3.

Due to the dependence on ε of the effective moduli introduced in Eq. (9), the interphase results to be characterized by a *soft* material (Rizzoni et al., 2014). Thereby, the interphase elastic moduli are linearly-rescaled with respect to the thickness ε as $\mathbb{C}^\varepsilon = \varepsilon\,\mathbb{C}$, where $\mathbb{C}^\varepsilon = \mathbb{S}^{-1}$ results from Eq. (9) and where the fourth-order tensor $\mathbb{C}$ does not depend on ε. Accordingly, the interphase constitutive law $\hat{\boldsymbol{\sigma}}^\varepsilon = \mathbb{C}^\varepsilon : \mathbf{e}(\hat{\mathbf{u}}^\varepsilon)$ can be recast within the asymptotic framework as

$$\hat{\boldsymbol{\sigma}}^0 + \varepsilon\,\hat{\boldsymbol{\sigma}}^1 = \mathbb{C} : (\hat{\mathbf{e}}^{-1} + \varepsilon\,\hat{\mathbf{e}}^0) + \mathrm{o}(\varepsilon) \tag{17}$$

previous equation having to be satisfied for any value of ε. Thereby, the following relationship holds

$$\hat{\boldsymbol{\sigma}}^0 = \mathbb{C} : (\hat{\mathbf{e}}^{-1}) \tag{18}$$

and, owing Eq. (14), it follows that

$$\hat{\boldsymbol{\sigma}}^0\,\mathbf{e}_3 = \mathbf{K}\,\hat{\mathbf{u}}^0_{,3} \tag{19}$$

where the matrix $\mathbf{K}$ is defined component-wise as $(\mathbf{K})_{ij} = (\mathbb{C})_{i3j3}$, and it results in $\mathbf{K} = \mathrm{diag}\left[K^{\mathcal{A}}_T \quad K^{\mathcal{A}}_T \quad K^{\mathcal{A}}_N\right]$ with

$$K^{\mathcal{A}}_T = \frac{3\,E_0\,\lambda^2(2-\nu_0)}{64\,b^3\,(1-\nu_0^2)}, \quad K^{\mathcal{A}}_N = \frac{3\,E_0\,\lambda^2}{32\,b^3\left(1-\nu_0^2\right)} \tag{20}$$

By integrating Eq. (19) with respect to z_3 from $-1/2$ to $+1/2$, and in the limit of ε tending to zero, the following zero-order soft-interface law is straight obtained

$$\mathbf{t}_3 = \mathbf{K}\,[\mathbf{u}], \quad [\mathbf{t}_3] = \mathbf{0} \quad \text{across } \mathcal{S} \tag{21}$$

where $[\,\cdot\,]$ denotes the jump across the interface.

As a result, quantities $K^{\mathcal{A}}_T$ and $K^{\mathcal{A}}_N$ introduced in Eq. (20) represent tangential and normal interface stiffnesses, respectively, associated to the auxiliary model problem $\mathcal{A}$. In particular, they depend on the effective elastic properties of the undamaged interphase, as well as on the characteristic length (namely, λ) of the plane region $\Delta\Omega^\varepsilon \cap \pi$ and on the microcrack radius b. It is worth remarking that, these quantities are introduced in the auxiliary problem $\mathcal{A}$ as descriptors of the microgeometry features in the contact problem $\mathcal{C}$, and they correspond to the average roughness wavelength and to the average no-contact radius, respectively.

2.3. Effective incremental contact stiffnesses

As a matter of fact, contact microgeometry and, in particular, the characteristic length of no-contact regions depend on the value of the nominal contact pressure $\bar{p}$. Thereby, for a given pressure condition characterizing the contact problem $\mathcal{C}(\bar{p})$, the corresponding auxiliary model problem $\mathcal{A}(\bar{p})$ is matched to the previous one by considering the microcracks radius b as dependent itself on $\bar{p}$, such that $0 \le 2\,b \le \lambda/\sqrt{2}$. In detail, in agreement with the approach proposed by Johnson et al. (1985) and Johnson (1987), $2\,b \le \lambda/\sqrt{2}$ when $\bar{p} < p^*$ and $b \to 0^+$ when $\bar{p} \to p^*$, where p^* is a measure of the nominal pressure which brings the surfaces into complete contact in $\mathcal{C}$, and referred to as the complete contact pressure.

In agreement with the Hertz elastic contact theory, an estimate for p^* in $\mathcal{C}$ can be defined as (Johnson et al., 1985):

$$p^*_H = \sqrt{2}\pi\,E'\,\frac{\Delta_0}{\lambda} \tag{22}$$

$(E')^{-1} = [(1-\nu_1^2)/E_1 + (1-\nu_2^2)/E_2]$ being the reduced Hertz modulus and Δ_0 being the amplitude of the bi-sinusoidal shape idealizing the contacting rough surfaces at the reference configuration.

It is worth observing that, Eq. (22) strictly holds in an elastic regime. Nevertheless, due to localization mechanisms associated to tips plastic deformation and fatigue effects, the pressure that brings the surfaces into a complete contact condition is surely lower than p^*_H and it can be considered as a function of the elasto-plastic material behavior, of the pressure loading history, as well as of the number of loading cycles. Accordingly, a possible description of the actual closure pressure can be postulated as:

$$p^* = h\,p^*_H = h\,\sqrt{2}\pi\,E'\,\frac{\Delta_0}{\lambda} \tag{23}$$

where $h \le 1$ is a suitable history-based correction term. In the case of loading cycles characterized by the same maximum value of the closure pressure, h can be retained in the order of Δ/Δ_0, where Δ is a measure of the amplitude for the wavy geometry that idealizes the contacting surfaces at the actual configuration.

Referring to the contact problem $\mathcal{C}$, the contact areas lying on $\mathcal{S}$ are described by introducing the average contact radius $a^{\mathcal{C}}$, such that $a^{\mathcal{C}} \to 0^+$ when $\bar{p} \to 0^+$ and $a^{\mathcal{C}} \to \lambda/\sqrt{2}$ when $\bar{p} \to p^*$. With reference to the sketch depicted in Fig. 2, and in agreement with both indications provided by Johnson et al. (1985) and numerical evidence by Yastrebov et al. (2014), when $\bar{p} \to 0^+$ then contact areas are described as circular (i.e., contact point condition)

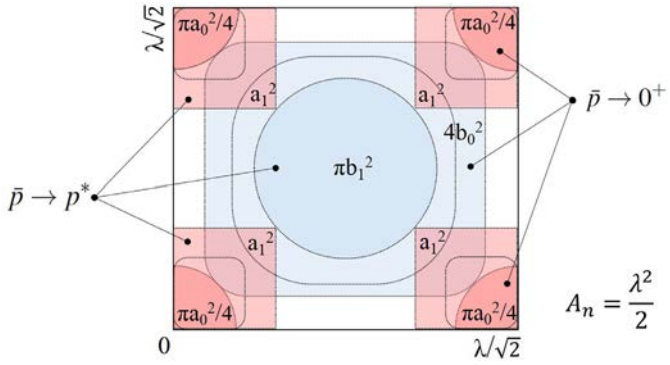

Fig. 2. Contact (light red) and no-contact (light blue) areas in $\Delta\Omega^{\varepsilon} \cap \pi \subset \mathcal{S}$. Outline of the simplified behavior modeled in the contact problem $\mathcal{C}$ for $\bar{p} \to 0^+$ and $\bar{p} \to p^*$. (For interpretation of the references to color in this figure legend, the reader is referred to the web version of this article.)

and no-contact areas are almost square-shaped. On the contrary, in the near complete closure condition ($\bar{p} \to p^*$), the contact areas are assumed to be almost square-shaped and the no-contact areas as quasi-circular.

Let a_0 and b_0 (respectively, a_1 and b_1) be the values of the contact and no-contact radii, respectively, when $\bar{p} \to 0^+$ (resp., $\bar{p} \to p^*$). In agreement with asymptotic estimates provided by Johnson et al. (1985), strictly valid for the elastic contact between a bi-sinusoidal surface and a rigid flat plane, the following relationships are assumed to hold:

$$a_0\left(\frac{\bar{p}}{p^*}\right) = \frac{\lambda}{\sqrt{2}}\left(\frac{3}{8\pi}\frac{\bar{p}}{p^*}\right)^{1/3} \tag{24}$$

$$b_0\left(\frac{\bar{p}}{p^*}\right) = \frac{\lambda}{2\sqrt{2}}\sqrt{1-\pi\left(\frac{3}{8\pi}\frac{\bar{p}}{p^*}\right)^{2/3}} \tag{25}$$

$$a_1\left(\frac{\bar{p}}{p^*}\right) = \frac{\lambda}{2\sqrt{2}}\sqrt{1-\frac{3}{2\pi}\left(1-\frac{\bar{p}}{p^*}\right)} \tag{26}$$

$$b_1\left(\frac{\bar{p}}{p^*}\right) = \frac{\lambda}{2\pi}\sqrt{3\left(1-\frac{\bar{p}}{p^*}\right)} \tag{27}$$

Therefore, contact (namely, $a^{\mathcal{C}}$) and no-contact ($b^{\mathcal{C}}$) radius evolution with $\bar{p}$ in $\mathcal{C}$ is postulated to be simply described by the following area-based weighted averages:

$$a^{\mathcal{C}}\left(\frac{\bar{p}}{p^*}\right) = \sqrt{\frac{\pi a_0^2\left(1-\frac{\bar{p}}{p^*}\right)+4a_1^2\frac{\bar{p}}{p^*}}{\pi\left(1-\frac{\bar{p}}{p^*}\right)+4\frac{\bar{p}}{p^*}}} \tag{28}$$

$$b^{\mathcal{C}}\left(\frac{\bar{p}}{p^*}\right) = \sqrt{\frac{4b_0^2\left(1-\frac{\bar{p}}{p^*}\right)+\pi b_1^2\frac{\bar{p}}{p^*}}{4\left(1-\frac{\bar{p}}{p^*}\right)+\pi\frac{\bar{p}}{p^*}}} \tag{29}$$

It is worth pointing out that, Eqs. (28) and (29) satisfy the consistency condition:

$$A_c + A_{nc} = A_n = \frac{\lambda^2}{2} \tag{30}$$

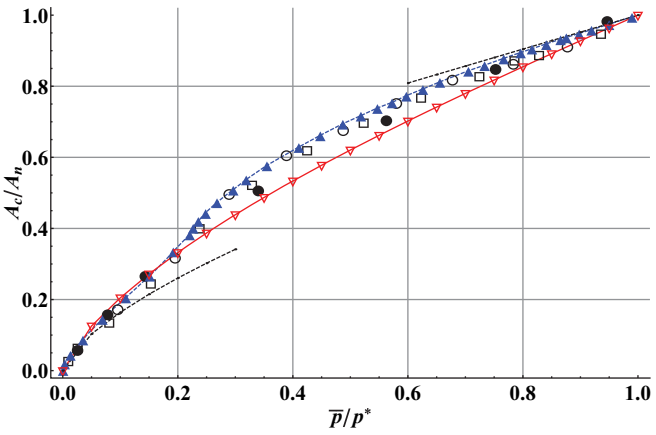

Fig. 3. Normalized contact area A_c/A_n versus the pressure ratio $\bar{p}/p^*$. □: Numerical results by Krithivasan and Jackson (2007). •: Experimental results by Johnson et al. (1985). ○: Numerical results by Johnson et al. (1985). −▲−: Numerical results by Yastrebov et al. (2014). − − −: Asymptotic limits by Johnson (1987). −▽−: Proposed analytical description (Eqs. (30) and (31)).

where the contact (A_c) and the no-contact (A_{nc}) area in $\Delta\Omega^{\varepsilon} \cap \pi$ are:

$$A_c = (a^{\mathcal{C}})^2\left[\pi\left(1-\frac{\bar{p}}{p^*}\right)+4\frac{\bar{p}}{p^*}\right] \tag{31}$$

$$A_{nc} = (b^{\mathcal{C}})^2\left[4\left(1-\frac{\bar{p}}{p^*}\right)+\pi\frac{\bar{p}}{p^*}\right] \tag{32}$$

Moreover, Eqs. (28) and (29) recover the asymptotic relationships introduced in Eqs. (24)–(27), and in particular the following limits for $\bar{p} \to 0^+$ hold:

$$a^{\mathcal{C}} \to a_0 \to \mathrm{O}\left(\left(\frac{\bar{p}}{p^*}\right)^{\frac{1}{3}}\right), \quad b^{\mathcal{C}} \to b_0 \to \frac{\lambda}{2\sqrt{2}} \tag{33}$$

In order to show consistency and accuracy of proposed estimates for contact and no-contact areas, the normalized contact area A_c/A_n computed via Eqs. (30) and (31) is successfully compared, in Fig. 3 and with respect to the dimensionless closure pressure $\bar{p}/p^*$, with: numerical results proposed by Krithivasan and Jackson (2007) and by Yastrebov et al. (2014), experimental data reported by Johnson et al. (1985), theoretical asymptotic limits provided by Johnson (1987). It appears that, although simple, the proposed approach can be retained effective for describing in a satisfactorily accurate way the evolution of the contact area versus $\bar{p}$. Accordingly, Eq. (29) can be considered as a suitable evolution law for the average no-contact radius $b^{\mathcal{C}}$ in $\mathcal{C}$.

By adopting $b = b^{\mathcal{C}}$ as the matching condition between the contact problem $\mathcal{C}(\bar{p})$ and the corresponding auxiliary model one $\mathcal{A}(\bar{p})$ for a given value of the nominal closure pressure, Eq. (29) can be employed in Eq. (20) for defining the interface stiffnesses resulting from the problem $\mathcal{A}$.

It is worth remarking that, Eq. (29) has not to be considered as governing the physical evolution of the crack-closing process induced by a closure pressure condition in the problem $\mathcal{A}$. Indeed, Eq. (29) furnishes a simple and physically-oriented description of the pressure-based evolution of the no-contact radius in $\mathcal{C}(\bar{p})$, adopted, for each value of $\bar{p}$, for defining the corresponding actual auxiliary model problem $\mathcal{A}(\bar{p})$.

Furthermore, Eq. (20) cannot be directly used as interfacial contact stiffnesses since, due to the limit conditions expressed in Eq. (33), stiffnesses introduced in Eq. (20) do not recover the physical behavior associated to null stiffness values when $\bar{p} \to 0^+$. Such an occurrence is described, for instance, by the Hertz theory.

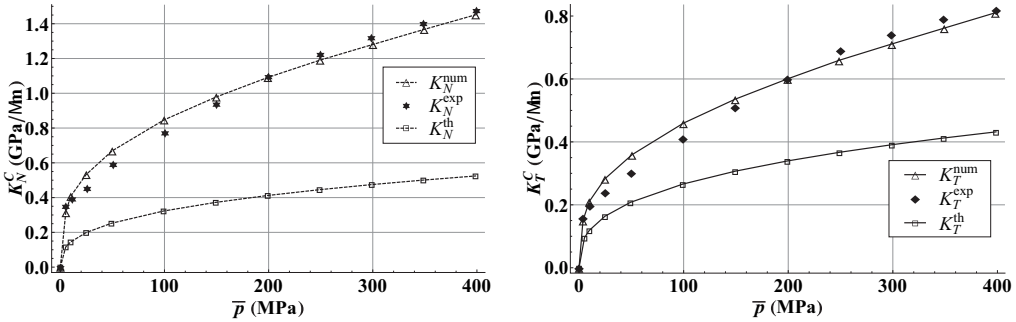

Fig. 4. Comparison between numerical (num, present model) and experimental (exp, Gonzalez-Valadez et al., 2010) results for normal (on the left) and tangential (on the right) contact stiffnesses vs. the nominal closure pressure $\bar{p}$. Hertz-based theoretical predictions (th, based on Eq. (34)) are also provided.

Indeed, in this case, theoretical estimates of interface contact stiffnesses can be expressed as (Sevostianov and Kachanov, 2008a)

$$K_N^{\text{th}} = \frac{4E'}{\lambda^2}\, a^{\mathcal{C}}\,, \qquad K_T^{\text{th}} = K_N^{\text{th}}\, \frac{2(1-\nu_0)}{(2-\nu_0)} \tag{34}$$

and therefore for $\bar{p} \to 0^+$ it results $\{K_N^{\text{th}}, K_T^{\text{th}}\} \to \mathrm{O}((\bar{p}/p)^{1/3})$.

In order to recover such a behavior for $\bar{p} \to 0^+$, the effective contact stiffnesses are recast as:

$$K_i^{\mathcal{C}} = K_i^{\mathcal{A}}\left[1 - \mathrm{e}^{-\gamma_i^0 \left(\frac{\bar{p}}{p^*}\right)^{1/3}}\right] \qquad i = N, T \tag{35}$$

where $K_N^{\mathcal{A}}$ and $K_T^{\mathcal{A}}$ are obtained from the imperfect interface approach, that is by Eq. (20), and γ_N^0 and γ_T^0 are model dimensionless parameters.

By enforcing that $K_i^{\mathcal{C}} = K_i^{\text{th}}$ when $\bar{p} \to 0^+$ (for $i = N, T$), the following theoretical estimates for γ^0-type model parameters can be obtained:

$$\gamma_{N,\text{th}}^0 = (9\pi)^{-1/3} \simeq 0.33\,, \qquad \gamma_{T,\text{th}}^0 = \gamma_{N,\text{th}}^0\, \frac{4(1-\nu_0)}{(2-\nu_0)^2} \tag{36}$$

with $\gamma_{T,\text{th}}^0 \simeq 0.32$ for $\nu_0 = 0.3$.

3. Results and discussion

In the following, some comparisons among model results and both experimental data available in literature and theoretical estimates are presented, aiming to validate the proposed approach and to show its soundness and effectiveness. Afterwards, the influence of the model parameters γ_N^0, γ_T^0 and h on the evolution of the interface contact stiffnesses introduced in Eq. (35) versus the closure pressure is investigated.

3.1. Model validation

The experimental results obtained by Gonzalez-Valadez et al. (2010) are herein chosen to validate the proposed model. In detail, they provided experimental measures, by means of ultrasonic pulser-receivers, of interface contact stiffnesses for steel specimens in contact through rough nominally-flat surfaces under a closure pressure. The specimens were subjected to loading-unloading cycles of compressive pressure in a hydraulic frame operating in loading control mode. The load was applied in a quasi-static way, up to the nominal-closure-pressure value of 400 MPa. Steel specimens were characterized by the following mechanical properties: $E_1 = E_2 = E_0 = 200$ GPa and $\nu_1 = \nu_2 = \nu_0 = 0.3$. Accordingly, Hertz-based reduced modulus value results in $E' = 109.89$ GPa. Moreover, in agreement with data furnished by Gonzalez-Valadez et al. (2010), contact rough surfaces in the reference configuration can be idealized as regularized wavy-shapes (see Fig. 1) characterized by $\lambda = 130$ μm and $\Delta_0 = 1.58$ μm.

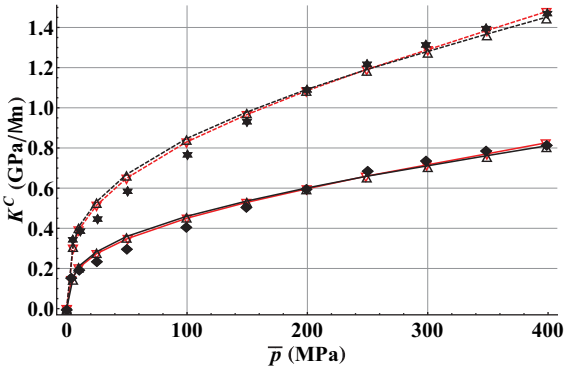

Fig. 5. Numerical (present model) and experimental (Gonzalez-Valadez et al., 2010) contact stiffnesses vs. the nominal closure pressure $\bar{p}$, computed considering: $p^* = p_H^*$ (i.e., for $h = 1$, the notation rule adopted in Fig. 4 applies), and a corrected complete contact pressure $p^* = 0.75\, p_H^*$ (i.e., for $h = 0.75$, - - ▽ - -: K_N^C; —▽—: K_T^C).

A comparison procedure among numerical results based on the proposed model and experimental data relevant to the 11-th loading cycle has been carried out, computing (via a least-squares fitting algorithm) the optimal values for parameters γ_N^0 and γ_T^0. As a result, the best-fitting values are $\gamma_{N,\text{num}}^0 = 0.96$ and $\gamma_{T,\text{num}}^0 = 0.58$, and the comparison between the corresponding results obtained via the proposed model and the available experimental data is depicted in Fig. 4.

It is worth pointing out that, the aforementioned numerical estimates for γ_N^0 and γ_T^0 are in the same order of magnitude of the corresponding Hertz-based theoretical ones (see Eq. (36)), and they clearly allow to obtain a good agreement with experimental data.

Previously results have been obtained by considering the complete contact pressure p^* as equal to the Hertz-based one p_H^* introduced in Eq. (22) (i.e., for $h = 1$). Nevertheless, by assuming as a coarse first approximation that $h = \Delta/\Delta_0$, and referring to the measures provided by Gonzalez-Valadez et al. (2010), the following estimates can be consistently considered: $\Delta = 1.18$ (at the 11-th loading cycle) and thereby $h = 0.75$. By adopting $p^* = 0.75\, p_H^*$, the numerical predictions of the contact stiffnesses remain in good agreement with the benchmark experimental results, as shown in Fig. 5, and in this case the best-fitting values of γ^0-parameters result in $\gamma_{N,\text{num}}^0 = 0.83$ and $\gamma_{T,\text{num}}^0 = 0.51$. Therefore, a history-based correction of the complete contact pressure leads to a consistent reduction of model parameters γ_N^0 and γ_T^0 towards their theoretical values.

Table 1 summarizes the best-fitting values of γ^0-type model parameters (normalized with respect to their Hertz-based theoretical predictions) for different values of the history parameter h. In detail, proposed results clearly show that a monotonic decrease of h induces a monotonic decrease of the best-fitting values for both

Table 1
Influence of the history-based correction quantity h on the best-fitting values (num) of the γ^0-type model parameters, normalized with respect to the theoretical (th) Hertz-based predictions.

h	0.15	0.2	0.25	0.3	0.35	0.4	0.5	0.75	1
$\gamma^0_{N,\text{num}}/\gamma^0_{N,\text{th}}$	0.7	1.0	1.2	1.4	1.6	1.8	2.0	2.5	2.9
$\gamma^0_{T,\text{num}}/\gamma^0_{T,\text{th}}$	0.5	0.7	0.8	0.9	1.0	1.1	1.3	1.6	1.8

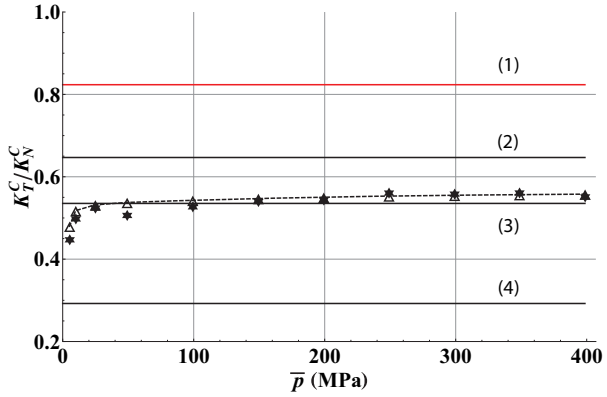

Fig. 6. Tangential-to-the-normal stiffness ratio vs. the nominal closure pressure $\bar{p}$. Comparison among present results (- - △ - -, computed with $p^* = p^*_H$) and both experimental (by Gonzalez-Valadez et al. (2010), ⋆) and theoretical predictions: (1) Mindlin (1949), (2) Sherif and Kossa (1991), (3) Baltazar et al. (2002), (4) Yoshioka and Scholz (1989). Results relevant to the model by Baltazar et al. (2002) have been computed considering $\xi = 0.65$ and $\kappa = 1$.

γ^0-type parameters, attaining the Hertz-based predictions differently for tangential and normal quantities. In all the corresponding cases the relative errors among model stiffness predictions and benchmarking experimental data remain always less than 12%.

Many studies on contacting rough surfaces (Greenwood and Williamson, 1966; Johnson et al., 1985; Krolikowski and Szczepek, 1993; Mindlin, 1949) revealed that the ratio of tangential-to-normal stiffness is solely dependent on the Poisson ratio of contacting materials. In those cases and under the assumption that the two bodies in contact are made by the same material, it results that:

$$\frac{K_T^C}{K_N^C} = \chi\,\phi(\nu) \tag{37}$$

where $0.5 \le \chi \le 2$ is a constant and $\phi(\nu)$ is a function of the Poisson ratio ν. In the case of the classic Hertz–Mindlin contact theory (Greenwood and Williamson, 1966; Krolikowski and Szczepek, 1993; Mindlin, 1949), $\chi = 2$ and $\phi(\nu) = (1-\nu)/(2-\nu)$. Many approaches are available in literature, providing relationships identical to that in Eq. (37), characterized by the same function $\phi(\nu)$ as in the Hertz–Mindlin theory but with different values of χ. Sherif and Kossa (1991) found $\chi = \pi/2$. Yoshioka and Scholz (1989) obtained the approximated estimate $\chi = 0.71$. Moreover, following the contact model by Baltazar et al. (2002), coefficient χ can be expressed as $\chi = \frac{2\xi}{\kappa}$, where ξ and κ are correction factors accounting for the geometrical misalignments with respect to shear and longitudinal directions, respectively. The resulting values of the tangential-to-normal stiffness ratio for the above cited models are plotted in Fig. 6, in comparison with the benchmarking experimental data (Gonzalez-Valadez et al., 2010) and with results obtained via the present model (referring to the best-fitting values of γ^0-type model parameters computed for $h = 1$).

It is worth noting that, the available experimental data suggest a significant dependence of the stiffness ratio on the closure pressure, especially for low values of $\bar{p}$. This is properly described by the proposed model, whereas the aforementioned theoretical predictions fail, providing a constant value of the ratio K_T^C/K_N^C, with a suitable description for values of $\bar{p}$ greater than 50 MPa only in the case of the formulation by Baltazar et al. (2002).

3.2. Comparison with the contact model by Sherif and Kossa

Sherif and Kossa (1991), and similarly Krolikowski and Szczepek (1993), in order to elucidate they experimental findings, provided a mathematical formulation of normal and tangential contact stiffnesses, by combining the contact model (GW) formulated by Greenwood and Williamson (1966) and the Hertz–Mindlin theory (Mindlin, 1949). In detail, contacting rough surfaces were modeled as elastic surfaces covered with elastic asperities which are assumed to be, at least near their summits, as spherical and characterized by the same radius of curvature R_s. Following Sherif and Kossa (1991) and their main references, the corresponding normal (denoted as K_N^{sk}) and tangential (K_T^{sk}) contact stiffnesses per unit area can be written in the form

$$K_N^{sk} = 2\,D_s\,\frac{E_0}{1-\nu_0^2}\,(R_s\sigma_s)^{\frac{1}{2}}\,F_{\frac{1}{2}}(t) \tag{38}$$

$$K_T^{sk} = \pi\,D_s\,\frac{E_0}{(2-\nu_0)(1+\nu_0)}\,(R_s\sigma_s)^{\frac{1}{2}}\,F_{\frac{1}{2}}(t) \tag{39}$$

where D_s is the density of asperities per unit area, σ_s is the standard deviation of the height distribution of asperities, t is the normalized (to σ_s) mean separation between contacting surfaces, and function $F_{\frac{1}{2}}(t)$ results in

$$F_{\frac{1}{2}}(t) = \int_t^\infty (r-t)^{\frac{1}{2}}\,\Theta(r)\,\mathrm{d}r \tag{40}$$

$\Theta(r)$ being defined as the height distribution, taken as Gaussian and scaled to make its standard deviation equal to the unity (Greenwood and Williamson, 1966).

In order to provide a consistent comparison among the proposed contact stiffnesses in Eq. (35), those recalled in Eqs. (38) and (39), and available experimental data by Gonzalez-Valadez et al. (2010), the normalized separation t is assumed to be dependent on the pressure ratio $\bar{p}/p^*$ and expressed by (Johnson et al., 1985):

$$t = 1 - \frac{\bar{p}}{p^*}\left[1 - \log\left(\frac{\bar{p}}{p^*}\right)\right] \tag{41}$$

Moreover, in agreement with the experimental characterization provided by Gonzalez-Valadez et al. (2010), stiffnesses in Eqs. (38) and (39) are computed by considering $E_0 = 200$ GPa, $\nu_0 = 0.3$, and by setting statistical parameters via the correlations given by McCool (1986): $R_s = 6.34\,\mu$m, $\sigma_s = 2\,\mu$m, $D_s = 7.32 \cdot 10^{-3}$ summits/μm^2.

Results proposed in Fig. 7 clearly highlight that the model herein proposed is much more effective than the statistical description adopted by Sherif and Kossa (1991) in reproducing benchmarking experimental data, both in terms of quantitative values of contact stiffnesses and as regards their evolution with respect the closure pressure, especially for small values of $\bar{p}$. In detail, proposed comparison confirms, in agreement with evidence provided by Buczkowski et al. (2014), that the model by Sherif and Kossa (1991) leads to underrated values of the incremental contact stiffnesses. Moreover, such a GW-based approach, contrary to the herein-proposed theoretical formulation, is not able to recover the pressure-dependent difference between normal and tangential stiffnesses, and thereby it is expected to be inaccurate in describing the tangential-to-normal stiffness ratio versus the closure pressure.

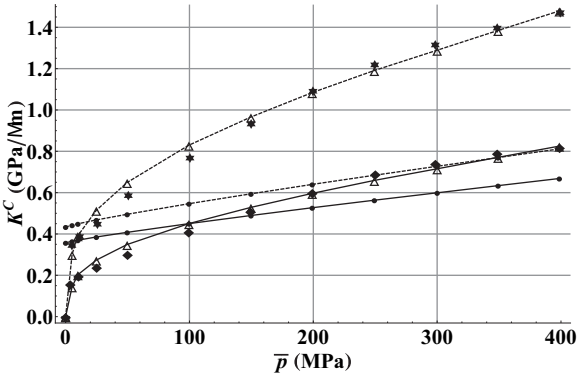

Fig. 7. Contact stiffnesses vs. the nominal closure pressure $\tilde{p}$. Comparison among: GW-based contact model by Sherif and Kossa (1991) (- - • - -: K_N^{sk}; –•–: K_T^{sk}), present approach (- - △ - -: K_N^C; –△–: K_T^C), and experimental results by Gonzalez-Valadez et al. (2010) (⋆: K_N^{exp}; ✦: K_T^{exp}).

3.3. Sensitivity analysis to main model parameters

A sensitivity analysis addressing the influence of both γ^0-type parameters and the history correction term h is herein focused, aiming to show how possible variations of model parameters with respect to their best-fitting values can affect the effectiveness of model predictions.

Fig. 8 shows normal and tangential stiffnesses, as well as the stiffness ratio K_T^C/K_N^C, versus the nominal closure pressure $\tilde{p}$, highlighting the comparison between model predictions and benchmarking experimental data (Gonzalez-Valadez et al., 2010) when γ^0-type model parameters differ from the corresponding best-fitting values of ±0.25% (in the case $h = 1$, i.e. for $p^* = p_H^*$). Moreover, Fig. 9 addresses the influence of the history parameter h on the stiffness predictions. Model results have been computed referring to the best-fitting values for γ^0-type parameters associated to the case $h = 1$.

As a general remark, possible variations of the history parameter h (for fixed optimal values of γ^0-type parameters) induce a reduced influence on the model capability to reproduce experimental results. On the contrary, a variation of γ^0-type parameters with respect to their best-fitting values can induce a certain influence on the evolution of the contact stiffnesses with the closure pressure. In detail, proposed results show that a variation of ±25% in γ^0-values produces a change in the slope of the incremental stiffnesses for small values of $\tilde{p}$, leading to differences with respect to the optimal predictions in the order of 15–25% (resp., 20–25%) for K_N^C (resp., for K_T^C) at $\tilde{p} = 400$ MPa. Besides, Fig. 8 highlights that the tangential-to-normal stiffness ratio evolution versus the nominal closure pressure exhibits a slight sensitivity to γ_N^0 and γ_T^0.

4. Conclusions

In the present paper a novel spring-like micromechanical contact model has been proposed. The microgeometry of two rough surfaces in no-sliding contact under a closure pressure has been assumed to be described by a distribution of *internal* penny-shaped cracks (namely, in the framework of internal-crack approaches), and the contact region has been modeled through a thin microcracked interphase separating the contacting bodies. Accordingly, the effective mechanical properties at the contact nominal interface are consistently derived by employing an imperfect interface approach (Fouchal et al., 2014; Rekik and Lebon, 2010, 2012), mainly based on two ingredients. On the first, the homogenization

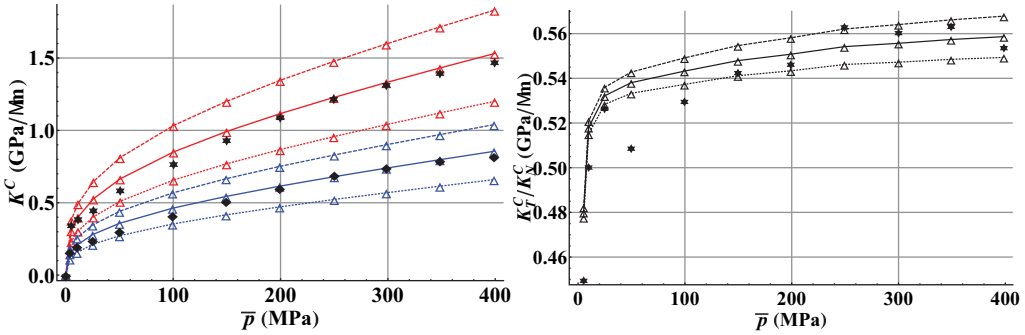

Fig. 8. Model sensitivity to parameters γ_N^0 and γ_T^0. Contact stiffnesses (on the left) and tangential-to-normal stiffness ratio (on the right). Best-fitting values $\gamma^0 = \gamma^*$ (——); $\gamma^0 = 1.25\gamma^*$ (– – –); $\gamma^0 = 0.75\gamma^*$ (· · · ·). On the left, red curves refer to K_N^C and blue ones to K_T^C. Experimental data by Gonzalez-Valadez et al. (2010) are also reported (⋆ and ✦, the notation rules adopted in Figs. 4 and 6 apply). (For interpretation of the references to color in this figure legend, the reader is referred to the web version of this article.)

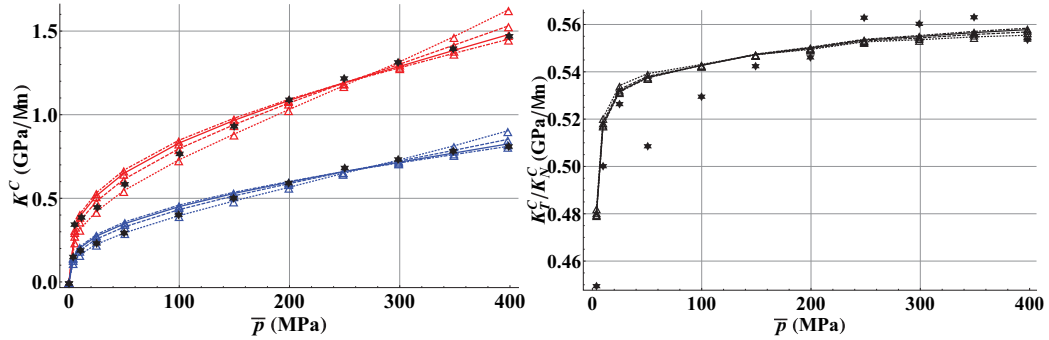

Fig. 9. Model sensitivity to the history parameter h. Contact stiffnesses (on the left) and tangential-to-normal stiffness ratio (on the right). $h = 0.3$ (· · · ·), $h = 0.5$ (– – –), $h = 0.75$ (——) and $h = 1$ (· – · – ·). On the left, red curves refer to K_N^C and blue ones to K_T^C. Experimental data by Gonzalez-Valadez et al. (2010) are also reported (⋆ and ✦, the notation rules adopted in Figs. 4 and 6 apply). (For interpretation of the references to color in this figure legend, the reader is referred to the web version of this article.)

of the interphase region has been performed by adopting the well-established strategy by Kachanov (1994), Tsukrov and Kachanov (2000), Kachanov and Sevostianov (2005) and Sevostianov and Kachanov (2013), under the assumption that cracks do not interact each other (non-interacting approximation). On the second, in the limit of a vanishing interphase thickness, a matched asymptotic expansion method (Lebon and Rizzoni, 2011; Lebon and Rizzoni, 2010; Lebon and Zaittouni, 2010; Rizzoni et al., 2014; Rizzoni and Lebon, 2013) has been considered. As a result, normal and tangential interface contact stiffnesses are consistently derived, introducing the dependency on the closure pressure $\bar{p}$ via a simple but accurate description for the evolution of the no-contact radius with $\bar{p}$, and by enforcing as consistency requirements some physical constraints suggested by the classical Hertz theory.

Results obtained via the present model have been compared to both theoretical predictions and available experimental data, highlighting soundness and effectiveness of the proposed approach. Moreover, the dependence of the contact stiffness ratio on the closure pressure has been successfully described, fully in agreement with the experimental evidence.

Model performance can be simply enhanced by including possible history-based effects, related to tips plastic deformation and fatigue behavior, by a proper setting of model parameters.

Although effective properties of contacting regions are usually derived by employing approaches based on *external* cracks (Sevostianov and Kachanov, 2008a; 2008b), internal-crack-based descriptions are proved to give reasonable results for normal contact compliance and electric resistance (Sevostianov, 2010). In this context, proposed results can be considered as an attempt to provide a more comprehensive insight on the effectiveness of internal-crack strategies in describing also tangential interface features for no-sliding contact under closure pressure conditions.

Acknowledgments

This work was supported by Bando Vinci 2013 (n. C2-73) of Università Italo-Francese UIF, and by Italian Civil Protection Department (RELUIS-DPC 2014-2018, CUP: E84G14000480007).

References

Baltazar, A., Rokhlin, S.I., Pecorari, C., 2002. On the relationship between ultrasonic and micromechanical properties of contacting rough surfaces. J. Mech. Phys. Solids 50 (7), 1397–1416.

Bristow, J.R., 1960. Microcracks, and the static and dynamic elastic constants of annealed and heavily cold-worked metals. Br. J. Appl. Phys. 11 (2), 81–85.

Buczkowski, R., Kleiber, M., Starzynski, G., 2014. Normal contact stiffness of fractal rough surfaces. Arch. Mech. 66 (6), 411–428.

Ciarlet, P.G., 1997, 27. Mathematical Elasticity (Volume II: Theory of Plates. Studies in Mathematics and its Applications). North-Holland, Amsterdam.

Dwyer-Joyce, R.S., Gonzalez-Valadez, M., 2003. Ultrasonic determination of normal and shear interface stiffness and the effect of Poisson's ratio. Tribol. Ser. 43, 143–149.

Eshelby, J.D., 1961. Elastic inclusions and inhomogeneities. Prog. Solid Mech. 2 (1), 89–140.

Fouchal, F., Lebon, F., Raffa, M.L., Vairo, G., 2014. An interface model including cracks and roughness applied to masonry. Open Civil Eng. J. 8, 263–271.

Gonzalez-Valadez, M., Baltazar, A., Dwyer-Joyce, R.S., 2010. Study of interfacial stiffness ratio of a rough surface in contact using a spring model. Wear 268 (3-4), 373–379.

Greenwood, J.A., Williamson, J.B., 1966. Contact of nominally flat surfaces. Proc. R. Soc. Lond. Ser. A 295 (1442), 300–319.

Johnson, K., 1987. Contact Mechanics. Cambridge University Press, Cambridge.

Johnson, K.L., Greenwood, J.A., Higginson, J.G., 1985. The contact of elastic regular wavy surfaces. Int. J. Mech. Sci. 27 (6), 383–396.

Kachanov, M., 1994. Elastic solids with many cracks and related problems. In: Hutchinson, J., Wu, T. (Eds.), Advances in Applied Mechanics, 30. Academic Press, New York, pp. 256–445.

Kachanov, M., Sevostianov, I., 2005. On quantitative characterization of microstructures and effective properties. Int. J. Solids Struct. 42 (2), 309–336.

Krithivasan, V., Jackson, R.L., 2007. An analysis of three-dimensional elasto-plastic sinusoidal contact. Tribol. Lett. 27 (1), 31–43.

Krolikowski, J., Szczepek, J., 1993. Assessment of tangential and normal stiffness of contact between rough surfaces using ultrasonic method. Wear 160 (2), 253–258.

Krolikowski, J., Szczepek, J., Witczak, Z., 1989. Ultrasonic investigation of contact between solids under high hydrostatic-pressure. Ultrasonics 27 (1), 45–49.

Lebon, F., Rizzoni, R., 2010. Asymptotic analysis of a thin interface: the case involving similar rigidity. Int. J. Eng. Sci. 48 (5), 473–486.

Lebon, F., Rizzoni, R., 2011. Asymptotic behavior of a hard thin linear elastic interphase: an energy approach. Int. J. Solids Struct. 48 (3-4), 441–449.

Lebon, F., Zaittouni, F., 2010. Asymptotic modelling of interfaces taking contact conditions into account: asymptotic expansions and numerical implementation. Int. J. Eng. Sci. 48 (2), 111–127.

McCool, J.I., 1986. Comparison of models for the contact of rough surfaces. Wear 107 (1), 37–60.

Mindlin, R.D., 1949. Compliance of elastic bodies in contact. J. Appl. Mech. 71, 259–268.

Nemat-Nasser, S., Hori, M., 2013. Micromechanics: Overall Properties of Heterogeneous Materials. Elsevier, Amsterdam.

Rekik, A., Lebon, F., 2010. Identification of the representative crack length evolution in a multi-level interface model for quasi-brittle masonry. Int. J. Solids Struct. 47 (22-23), 3011–3021.

Rekik, A., Lebon, F., 2012. Homogenization methods for interface modeling in damaged masonry. Adv. Eng. Softw. 46 (1), 35–42.

Rizzoni, R., Dumont, S., Lebon, F., Sacco, E., 2014. Higher order model for soft and hard elastic interfaces. Int. J. Solids Struct. 51 (23–24), 4137–4148.

Rizzoni, R., Lebon, F., 2013. Imperfect interfaces as asymptotic models of thin curved elastic adhesive interphases. Mech. Res. Commun. 51, 39–50.

Sanchez-Palencia, E., 1980. Non-Homogeneous Media and Vibration Theory. Lecture Notes in Physics, 127. Springer, Berlin Heidelberg.

Sanchez-Palencia, E., Sanchez-Hubert, J., 1992. Introduction Aux Méthodes Aymptotiques et à l' Homogénéisation: Application à la Mécanique des Milieux continous. Masson, Paris.

Sanchez-Palencia, E., 1987. General introduction to asymptotic methods. In: Sanchez-Palencia, E., Zaoui, A. (Eds.), Homogenization Techniques for Composite Media. In: Lecture Notes in Physics, 272. Springer, Berlin Heidelberg, pp. 121–136.

Sevostianov, I., 2010. Incremental elastic compliance and electric resistance of a cylinder with partial loss in the cross-sectional area. Int. J. Eng. Sci. 48 (6), 582–591.

Sevostianov, I., Kachanov, M., 2008a. Contact of rough surfaces: a simple model for elasticity, conductivity and cross-property connections. J. Mech. Phys. Solids 56 (4), 1380–1400.

Sevostianov, I., Kachanov, M., 2008b. Normal and tangential compliances of interface of rough surfaces with contacts of elliptic shape. Int. J. Solids Struct. 45, 2723–2736.

Sevostianov, I., Kachanov, M., 2013. Non-interaction approximation in the problem of effective properties. In: Kachanov, M., Sevostianov, I. (Eds.), Effective Properties of Heterogeneous Materials. Solid Mechanics and its Applications, 193. Springer, Dordrecht, pp. 1–95.

Sherif, H.A., Kossa, S.S., 1991. Relationship between normal and tangential contact stiffness of nominally flat surfaces. Wear 151 (1), 49–62.

Temizer, I., Wriggers, P., 2011. Homogenization in finite thermoelasticity. J. Mech. Phys. Solids 59 (2), 344–372.

Tsukrov, I., Kachanov, M., 2000. Effective moduli of an anisotropic material with elliptical holes of arbitrary orientational distribution. Int. J. Solids Struct. 37 (41), 5919–5941.

Westergaard, H., 1939. Bearing pressures and cracks. J. Appl. Mech. 6, A 49–53.

Yastrebov, V.A., Anciaux, G., Molinari, J.-F., 2014. The contact of elastic regular wavy surfaces revisited. Tribol. Lett. 56 (1), 171–183.

Yoshioka, N., Scholz, C.H., 1989. Elastic properties of contacting surfaces under normal and shear loads: 1 Theory. J. Geophys. Res. Solid Earth (1978–2012) 94 (B12), 17681–17690.